

Reverse electrical remodeling in rats with heart failure and preserved ejection fraction

Jae Hyung Cho, ... , Eduardo Marbán, Eugenio Cingolani

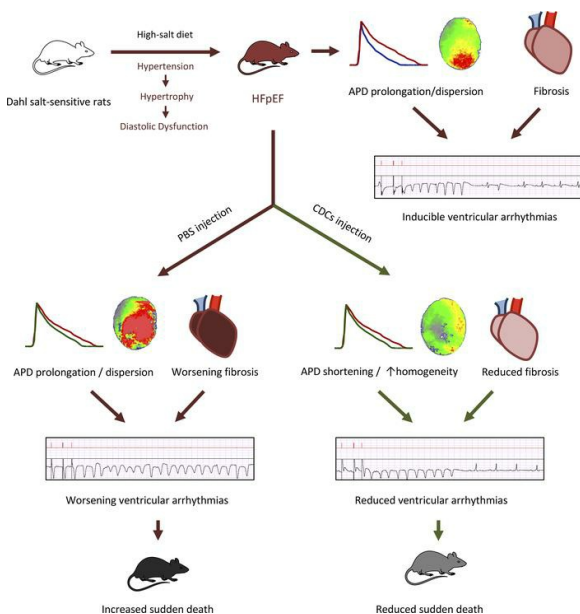
JCI Insight. 2018;3(19):e121123. <https://doi.org/10.1172/jci.insight.121123>.

Research Article

Cardiology

Stem cells

Graphical abstract



Find the latest version:

<https://jci.me/121123/pdf>



Reverse electrical remodeling in rats with heart failure and preserved ejection fraction

Jae Hyung Cho,¹ Peter J. Kilfoil,¹ Rui Zhang,¹ Ryan E. Solymani,¹ Catherine Bresee,² Elliot M. Kang,¹ Kristin Luther,¹ Russell G. Rogers,¹ Geoffrey de Couto,¹ Joshua I. Goldhaber,¹ Eduardo Marbán,¹ and Eugenio Cingolani¹

¹Smidt Heart Institute, Cedars-Sinai Medical Center, Los Angeles, California, USA. ²Biostatistics and Bioinformatics Research Center, Cedars-Sinai Medical Center, Los Angeles, California, USA.

Sudden death is the most common mode of exodus in patients with heart failure and preserved ejection fraction (HFpEF). Cardiosphere-derived cells (CDCs) reduce inflammation and fibrosis in a rat model of HFpEF, improving diastolic function and prolonging survival. We tested the hypothesis that CDCs decrease ventricular arrhythmias (VAs) and thereby possibly contribute to prolonged survival. Dahl salt-sensitive rats were fed a high-salt diet to induce HFpEF. Allogeneic rat CDCs (or phosphate-buffered saline as placebo) were injected in rats with echo-verified HFpEF. CDC-injected HFpEF rats were less prone to VA induction by programmed electrical stimulation. Action potential duration (APD) was shortened, and APD homogeneity was increased by CDC injection. Transient outward potassium current density was upregulated in cardiomyocytes from CDC rats relative to placebo, as were the underlying transcript (*Kcnd3*) and protein (Kv4.3) levels. Fibrosis was attenuated in CDC-treated hearts, and survival was increased. Sudden death risk also trended down, albeit nonsignificantly. CDC therapy decreased VA in HFpEF rats by shortening APD, improving APD homogeneity, and decreasing fibrosis. Unlike other stem/progenitor cells, which often exacerbate arrhythmias, CDCs reverse electrical remodeling and suppress arrhythmogenesis in HFpEF.

Introduction

Heart disease is the leading cause of death in the United States, accounting for approximately 600,000 deaths per year (1). Heart failure (HF) is second only to coronary artery disease as a cause of heart disease-related mortality (1), and clearly the two overlap considerably. Patients with HF have a poor prognosis, with a median survival of 2.1 years and 5-year mortality of 75% regardless of ejection fraction (EF) (2). Most advances in the therapy of HF over the last decades have been in HF with reduced EF (HFrEF) (3, 4), where various medications and implantable devices have prolonged life (4). The diastolic counterpart, HF with preserved EF (HFpEF), has attracted increasing attention recently due to the aging population with hypertension, diabetes mellitus, and obesity, all of which are common HFpEF comorbidities (5, 6). HFpEF now accounts for roughly half of all HF and its incidence continues to increase (5). Unlike HFrEF, clinical trials using β -blockers, angiotensin-converting enzyme inhibitors, angiotensin receptor blockers, and mineralocorticoid inhibitors have failed to prolong life in HFpEF patients (7). Inflammation and subsequent fibrosis figure prominently in the pathogenesis of HFpEF, although details remain sketchy (6–8). Sudden death is the most common mode of mortality in patients with HFpEF, accounting for approximately 25% of all deaths (9, 10). While the etiology of sudden death in HFpEF is poorly understood, ventricular arrhythmias (VAs) have been implicated in HFrEF (11). Dahl salt-sensitive (DSS) rats with echocardiographically verified HFpEF are at increased risk of inducible VA due to delayed repolarization and increased fibrosis (12). This is consistent with our previous findings using ambulatory electrocardiographic monitoring of HFpEF rats revealing development of spontaneous VA (13). HFpEF rats were observed dying suddenly and the sudden deaths were precipitated by spontaneous VA (13). In the same model of HFpEF, cardiosphere-derived cells (CDCs) markedly decrease inflammation and fibrosis, thereby reversing diastolic dysfunction and prolonging survival (8). These progenitor cells are already in clinical testing for HFpEF (Regress-HFpEF, clinicaltrials.gov/show/NCT02941705). Here, we investigate whether CDCs can reduce VA in HFpEF rats, and thereby possibly contribute to prolonged survival.

Conflict of interest: EM owns founder's equity in Capricor Inc.

Submitted: March 16, 2018

Accepted: August 21, 2018

Published: October 4, 2018

Reference information:

JCI Insight. 2018;3(19):e121123.

<https://doi.org/10.1172/jci.insight.121123>.

insight.121123.

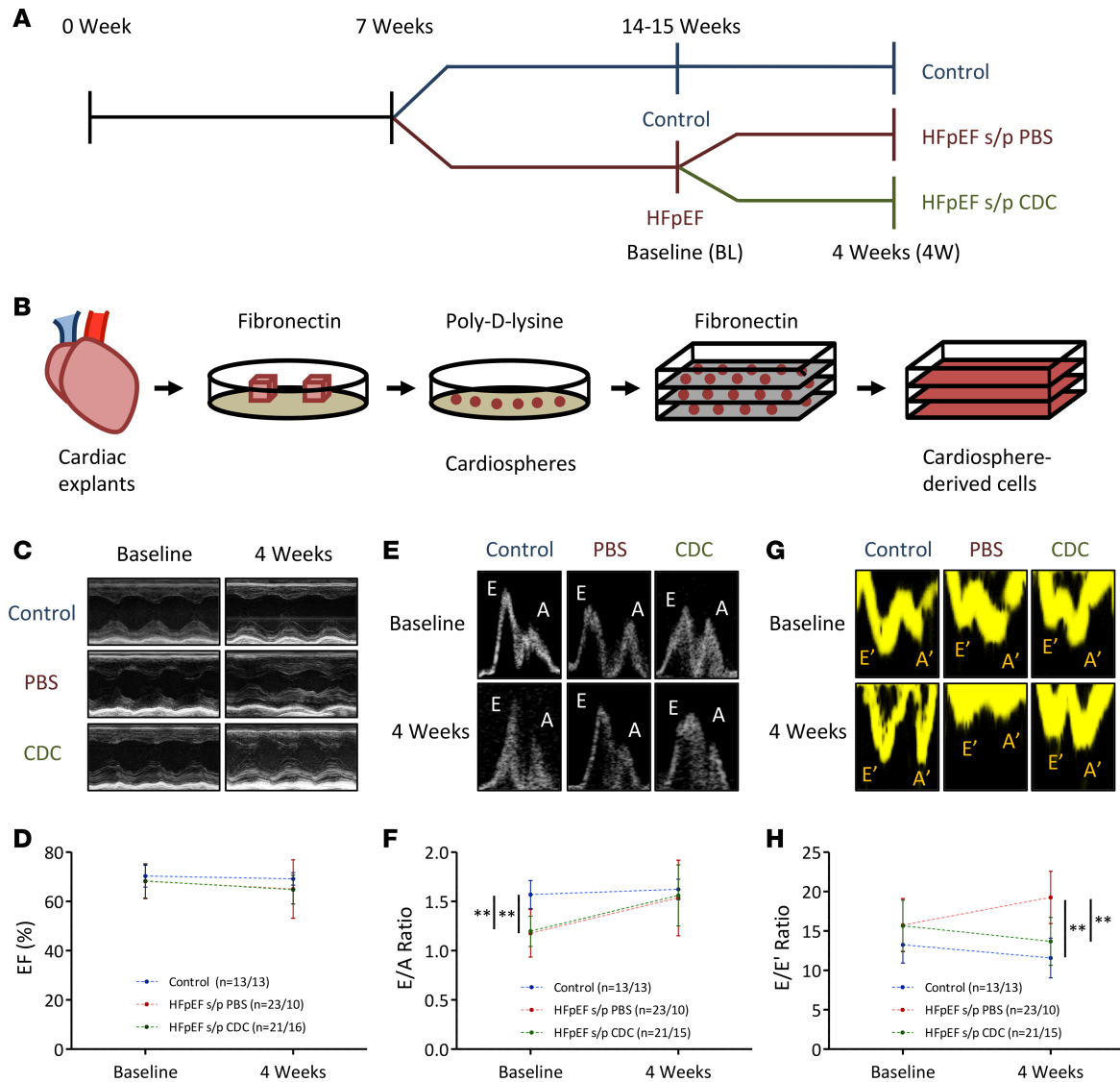


Figure 1. Experimental protocol, generation of CDCs, and echocardiographic measurement of systolic and diastolic function. (A) DSS rats were fed HS or NS diet from 7 weeks of age. At 14–15 weeks of age, baseline echocardiography was performed to assess EF, E/A, and E/E' ratios. HS rats with diastolic dysfunction, preserved EF, and objective HF signs were diagnosed with HFpEF. PES was performed and arrhythmogenic HFpEF rats were randomly assigned to intracoronary injection of CDCs versus PBS. Follow-up experiments were performed 4 weeks after the injection. (B) Allogeneic CDCs were generated from cardiac explant from a Sprague Dawley rat as described in the Methods. CDCs from passages 4–6 were used for injection. (C) Representative M-mode of parasternal short axis views of transthoracic echocardiography. (D) EF was preserved 4 weeks after injection in both groups (65% ± 6% in CDCs vs. 65% ± 12% in PBS, $P = 0.41$). (E) Representative E/A ratio from pulse wave Doppler at the mitral level. (F) Both CDC- and PBS-injected rats normalized E/A ratio 4 weeks after injection (1.56 ± 0.31 in CDCs vs. 1.54 ± 0.38 in PBS, $P = 0.99$). (G) Representative E/E' ratio from tissue Doppler imaging. (H) E/E' ratio of CDC-injected rats was decreased compared with PBS-injected rats (13.7 ± 3.0 in CDCs vs. 19.2 ± 3.5 in PBS, $P < 0.001$), which verified the improvement in diastolic function. ** $P < 0.001$. Error line indicates mean and standard deviation. Control rats were $n = 13$ at baseline and 4-week follow-up. PBS-injected HFpEF rats were $n = 23$ at baseline and $n = 10$ at 4 weeks. CDC-treated HFpEF rats were $n = 21$ at baseline and $n = 15$ –16 at 4 weeks. Mixed-model regression was used for D, F, and H.

Results

Reversal of diastolic dysfunction. DSS rats (7 weeks old) were fed high-salt (HS) diet to induce HFpEF (Figure 1A). DSS rats fed normal-salt (NS) diet served as controls. Echocardiography was performed at 14–15 weeks of age to assess systolic and diastolic function. Decreased E/A ratio, increased E/E' ratio, and normal EF are echocardiographic characteristics of HFpEF. Echo-verified HS-fed rats with signs of HF were diagnosed with HFpEF by 14–15 weeks of age. Programmed electrical stimulation (PES) was performed to assess propensity to VA at baseline; if noninducible, rats (4 of 48, 8.3%) were excluded from the study. Arrhythmogenic HFpEF rats were randomly assigned to intracoronary injection of CDCs versus placebo

(phosphate-buffered saline, PBS) (Figure 1A). Allogeneic CDCs were generated from a Sprague Dawley rat (Figure 1B) as described previously (14). Follow-up echocardiography was performed 4 weeks after injection to measure systolic and diastolic function. EF remained greater than 60%, confirming preserved systolic function (Figure 1, C and D). The ratio of the early (E) to late (A) ventricular filling velocities (E/A ratio) was normalized in both CDC and placebo groups (Figure 1, E and F), but E/A ratio alone cannot differentiate between progression of HFpEF (pseudonormal pattern) versus regression/reversal of diastolic dysfunction (15). To make this distinction, we measured an additional parameter of diastolic function, E/E' (ratio between the early mitral inflow velocity and mitral annular early diastolic velocity), which does not pseudonormalize as HFpEF worsens (15). Interestingly, while diastolic dysfunction progressed in placebo-treated rats, CDC-treated rats showed regression of diastolic dysfunction (Figure 1, G and H). Left atrial size was increased in HFpEF rats compared with controls by 14–15 weeks of age and subsequently decreased in CDC-injected rats compared with PBS-injected controls (Supplemental Figure 1A; supplemental material available online with this article; <https://doi.org/10.1172/jci.insight.121123DS1>). The E' wave was decreased in HFpEF rats compared with controls by 14–15 weeks of age and improved in CDC-treated rats compared with PBS-injected controls; however, this did not reach statistical significance (Supplemental Figure 1B). The reversal of diastolic dysfunction by CDCs confirms previous findings (8).

Decreased ventricular arrhythmogenesis in HFpEF rats. HFpEF rats are at increased risk of inducible VA (12), but the effects of CDCs on arrhythmogenesis have not been characterized. Follow-up PES was performed 4 weeks after the injection of CDCs or PBS, and compared for differences in arrhythmogenicity. The arrhythmogenicity index (AI), a heuristic measure of VA inducibility calculated as $([\text{number of VA beats}] + [\text{last stimulus coupling interval \{millisecond\} - 40}]) / (\text{square root of } [\text{number of extrastimuli}])$ (12), was markedly reduced in CDC-injected HFpEF rats compared with placebo rats (Figure 2, A and B). Among the components of AI, the number of VA beats (duration of the arrhythmia) was markedly reduced in CDC-treated animals compared with placebo rats (Figure 2C). The last extrastimulus coupling interval showed a trend towards reduction in CDC-treated rats compared with PBS, indicating the need for a more aggressive protocol to induce VA in the CDC group (Figure 2D). However, the number of extrastimuli did not reveal any differences (Supplemental Figure 1C).

Electrocardiographic changes of HFpEF rats. Surface electrocardiography (ECG) was used to assess the potential of CDCs to modify conduction or repolarization. QT interval, which measures repolarization, was shortened in CDC-treated rats compared with placebo rats (Figure 3, A and B), as was QTc interval (Figure 3C). However, PR interval (a measure of AV nodal conduction) and QRS duration were similar in CDC and PBS groups (Figure 3, D and E). Heart rate (measured by the RR interval) did not differ between the 2 groups (Figure 3F). The intrinsic deflection time did not change in CDC and PBS groups (Supplemental Figure 1D). Taken together, these findings suggest that CDC treatment of HFpEF rats abbreviated repolarization, which is prolonged in HFpEF (12, 16), while having no detrimental effects on AV nodal conduction or ventricular depolarization.

Action potential remodeling. To further investigate the repolarization remodeling induced by CDCs, we performed ex vivo optical mapping. Action potential duration (APD) was measured from 10 different areas of the left ventricle in the various experimental groups (Figure 3G). Average APD90 (APD at 90% repolarization) was reduced in CDC-treated animals compared with placebo-injected rats (Figure 3, H and I). Furthermore, APD dispersion (measured from the standard deviation of APD90) was improved in CDC compared with placebo rats (Figure 3, J and K). Both the observed reduction in APD90 and the increased repolarization homogeneity are antiarrhythmic effects that could potentially prevent VA in HFpEF.

Ionic current modulation. The cellular mechanisms of APD shortening and increased homogeneity exerted by CDC therapy were investigated by whole-cell patch clamp. APD prolongation in HFpEF rats is due to downregulation of the primary repolarizing current, the transient outward potassium current (I_{to}) (12). Although the rapid component of the delayed-rectifier potassium current (I_{Kr}) and the inward-rectifier potassium current (I_{K1}) were also reduced in HFpEF hearts, the contribution of these currents to overall APD in rats is far less than that of I_{to} (12). Here, we found that CDCs upregulated I_{to} density in HFpEF rats compared with placebo (Figure 4, A and B). Other minor repolarizing currents, i.e., I_{Kr} (Figure 4, C and D) and I_{K1} (Figure 4, E and F), were not affected by CDC therapy. Thus, an enhancement of I_{to} by CDCs underlies the abbreviation of APD in HFpEF rats.

Transcript and protein expression of ion channels. Transcript levels of I_{to} -encoding *Kcnd3* (Figure 5A) and the corresponding protein product, Kv4.3, were upregulated by CDC therapy (Figure 5, B and C). However, the genes for I_{Kr} (*Kcnh2*) and I_{K1} (*Kcnj2*) were not affected (Figure 5, D and G) nor were the corresponding proteins, Kv11.1

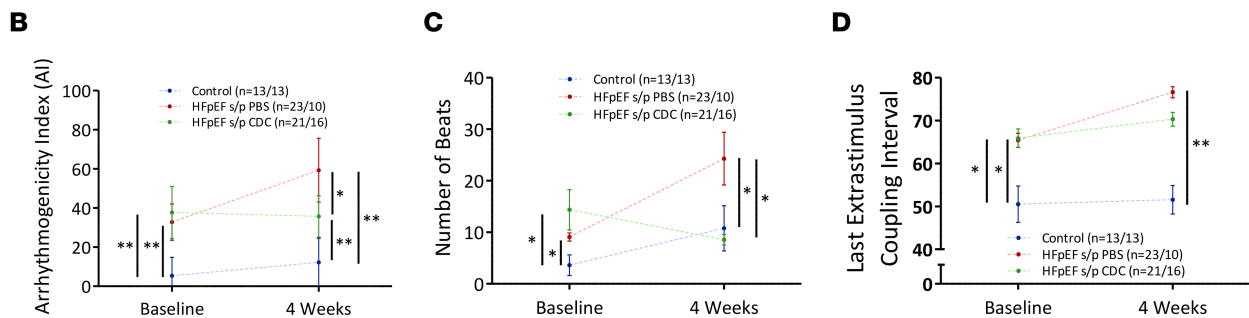
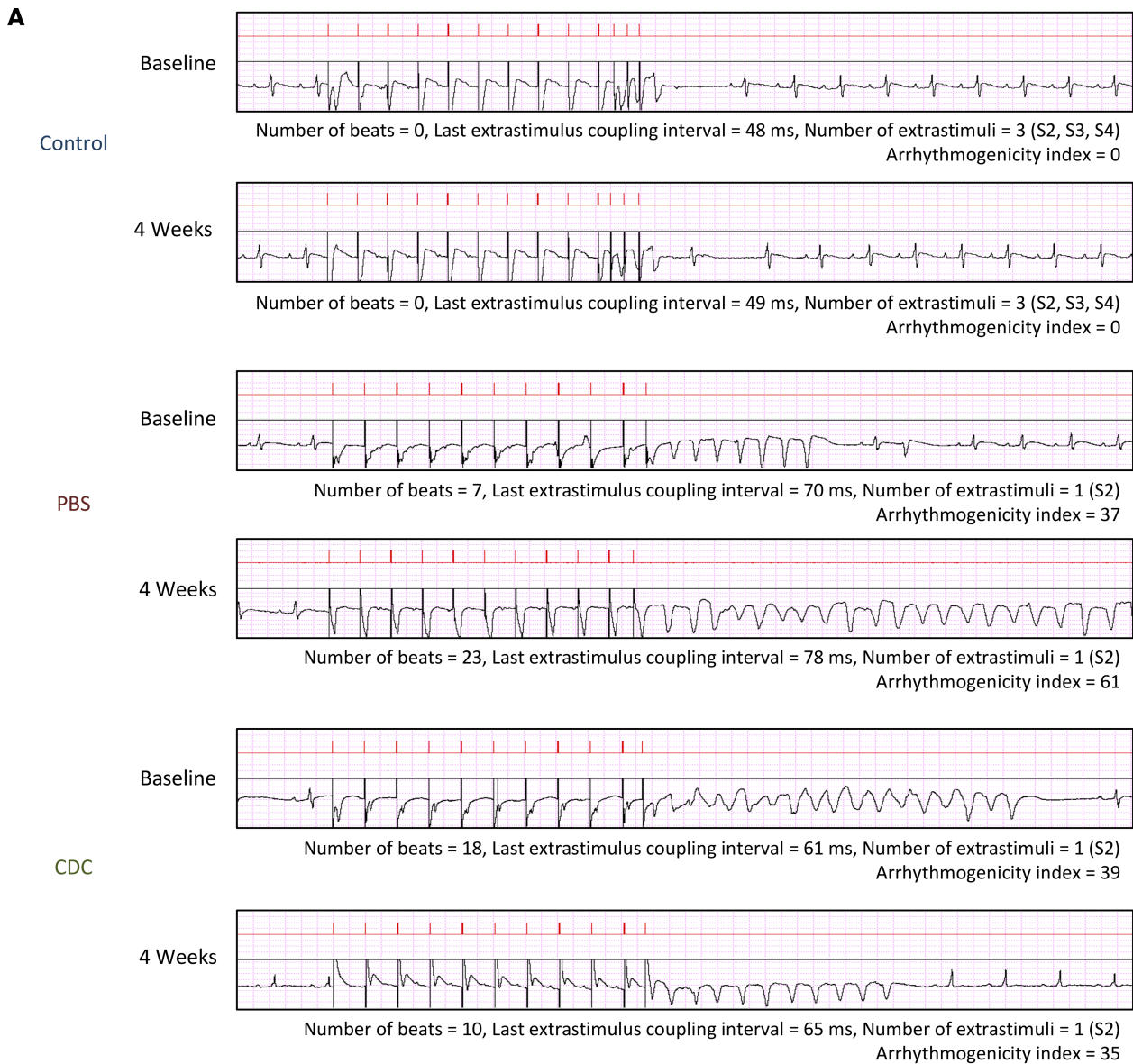


Figure 2. Antiarrhythmic effects of CDCs in HFpEF rats. (A) Representative PES records (upper panel, stimuli; lower panel, ECG) in control and HFpEF rats. **(B)** AI was decreased in CDC-treated rats compared with placebo-treated rats (36 ± 11 in CDCs vs. 61 ± 17 in PBS, $P = 0.025$). **(C)** Number of beats was decreased in CDC rats compared with placebo rats (9 ± 4 in CDCs vs. 24 ± 16 in PBS, $P = 0.018$). **(D)** The last extrastimulus coupling interval showed a nonsignificant trend towards reduction in CDC-treated rats (70 ± 7 ms in CDCs vs. 77 ± 4 ms in PBS, $P = 0.10$). * $P < 0.05$, ** $P < 0.001$. Error line indicates mean and standard deviation. Control rats were $n = 13$ at baseline and 4-week follow-up. PBS-injected HFpEF rats were $n = 23$ at baseline and $n = 10$ at 4 weeks. CDC-treated HFpEF rats were $n = 21$ at baseline and $n = 16$ at 4 weeks. Mixed-model regression was used for **B-D**.

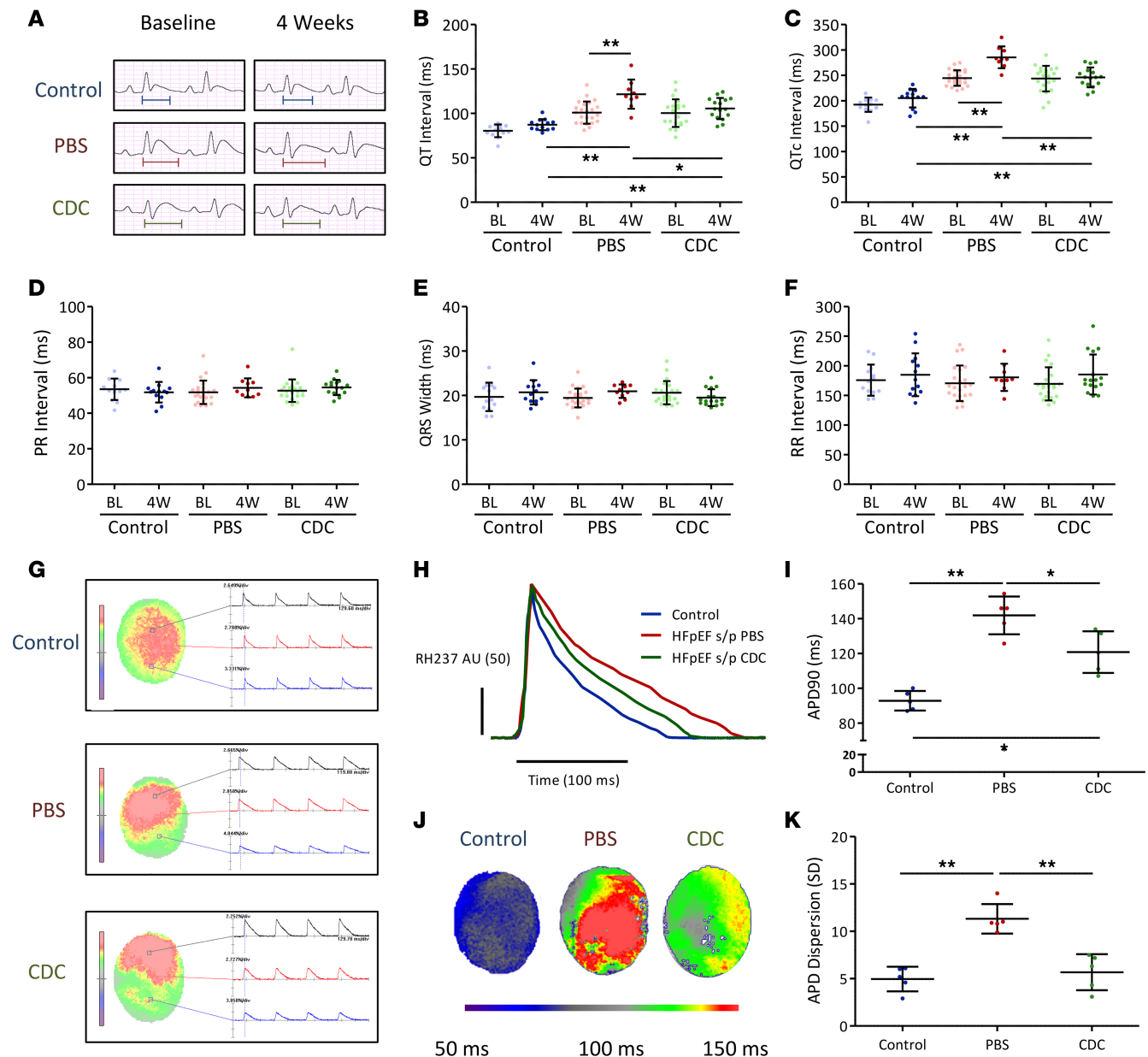


Figure 3. Electrocardiographic analyses and reverse electrophysiologic remodeling of action potential prolongation and dispersion. (A) Representative ECGs showing QT intervals in control, CDC, and PBS rats. (B) QT interval was decreased in CDC-treated HFpEF rats compared with PBS-injected rats (105.5 ± 11.8 ms in CDCs vs. 121.6 ± 16.2 ms in PBS, $P = 0.025$). (C) QTc interval was also decreased in CDC animals (246.1 ± 19.5 ms in CDCs vs. 285.5 ± 20.0 ms in PBS, $P < 0.001$). (D) PR interval was not changed (54.5 ± 4.3 ms in CDCs vs. 54.3 ± 5.3 ms in PBS, $P = 0.68$). (E) QRS duration did not change (19.5 ± 1.9 ms in CDCs vs. 21.0 ± 1.5 ms in PBS, $P = 0.87$). (F) RR interval was similar in both groups (185.4 ± 33.8 ms in CDCs vs. 180.7 ± 23.0 ms in PBS, $P = 0.84$). $*P < 0.05$, $**P < 0.001$. Error line indicates mean and standard deviation. Control rats were $n = 13$ at baseline and 4-week follow-up. PBS-injected HFpEF rats were $n = 23$ at baseline and $n = 10$ at 4 weeks. CDC-treated HFpEF rats were $n = 21$ at baseline and $n = 16$ at 4 weeks. Mixed-model regression was used for B–F. (G) Representative ex vivo optical mapping images of control and HFpEF hearts. (H) Representative action potential graphs of control, CDC-, and PBS-injected HFpEF rats. (I) APD90 was significantly reduced in CDC-treated rats compared with placebo rats (120.8 ± 11.9 ms in CDCs vs. 141.9 ± 10.9 ms in PBS, $P = 0.014$). (J) Representative APD map of control, CDC, and PBS rats. (K) The standard deviation of APD90 (APD90 dispersion) was significantly decreased in CDC rats compared with PBS rats (5.7 ± 1.9 in CDCs vs. 11.3 ± 1.6 in PBS, $P = 0.0003$). $*P < 0.05$, $**P < 0.001$. Error line indicates mean and standard deviation. $n = 5$ for each group. Kruskal-Wallis test was used for I and K.

(Figure 5, E and F) and Kir 2.1 (Figure 5, H and I). These changes at the transcript and protein levels mirror those found in ionic currents. Other proteins regulating I_{to} currents, such as Kv4.2, Kv1.4, and KChIP2 were checked; however, their expression levels were unchanged (Supplemental Figure 2). Connexin 43 expression was also checked and did not reveal any differences (Supplemental Figure 3). Hence, our findings are consistent with, but do not prove, the hypothesis that the CDC-related upregulation of I_{to} is transcriptionally mediated.

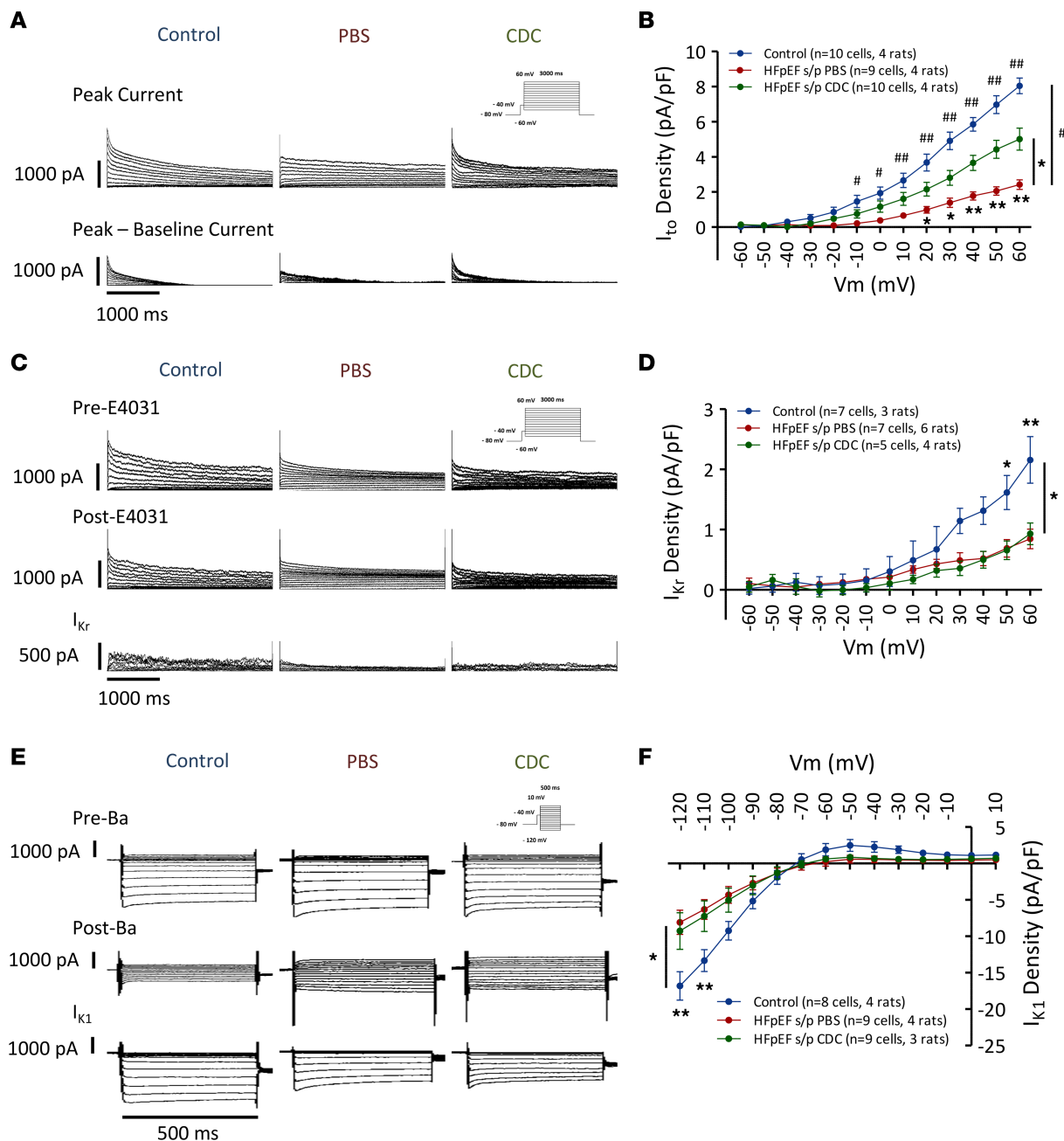


Figure 4. Upregulation of I_{to} and conserved I_{Kr} and I_{K1} . (A) Representative I_{to} records in control, CDC, and PBS cardiomyocytes. Peak minus baseline current is shown after subtraction. (B) I_{to} density was upregulated in CDC-treated cardiomyocytes compared with PBS cardiomyocytes (5.00 ± 1.98 in CDCs vs. 2.41 ± 0.82 pA/pF at 60 mV in PBS, $P < 0.001$). (C) Representative I_{Kr} recordings in control, CDC, and PBS rats. I_{Kr} is measured as E4031-sensitive current. (D) I_{Kr} density was unchanged in CDC and PBS animals (0.93 ± 0.40 in CDCs vs. 0.84 ± 0.43 pA/pF at 60 mV in PBS, $P > 0.99$). (E) Representative I_{K1} recordings in control, CDC, and PBS rats. Barium-sensitive current was measured as I_{K1} . (F) I_{K1} density was similar in CDC and PBS cardiomyocytes (-9.27 ± 7.52 in CDCs vs. -8.08 ± 4.98 pA/pF at -120 mV in PBS, $P > 0.99$). * $P < 0.05$, ** $P < 0.001$ (control vs. PBS); # $P < 0.05$, ## $P < 0.001$ (CDCs vs. PBS). Error line indicates mean and standard error of mean. Rat and cell numbers are shown in each figure. ANOVA was used for B, D, and F.

Attenuated fibrosis and increased survival. Myocardial fibrosis was quantified by Masson's trichrome staining. The extent of fibrosis was reduced by CDC therapy, a change which would favor APD homogeneity in HFpEF rats (Figure 6, A and B). HFpEF rats showed prolonged survival after CDC therapy at 14–15 weeks of age compared with placebo rats (Figure 6C). Survival analysis showed that CDC therapy decreased overall mortality (sudden death, seizure, and protocol-mandated euthanasia due to severe distress) (Figure 6D). Importantly, CDC therapy reduced sudden death from 17.4% to 9.5%, although this was not statistically significant, likely due to the low number of overall events in this limited population.

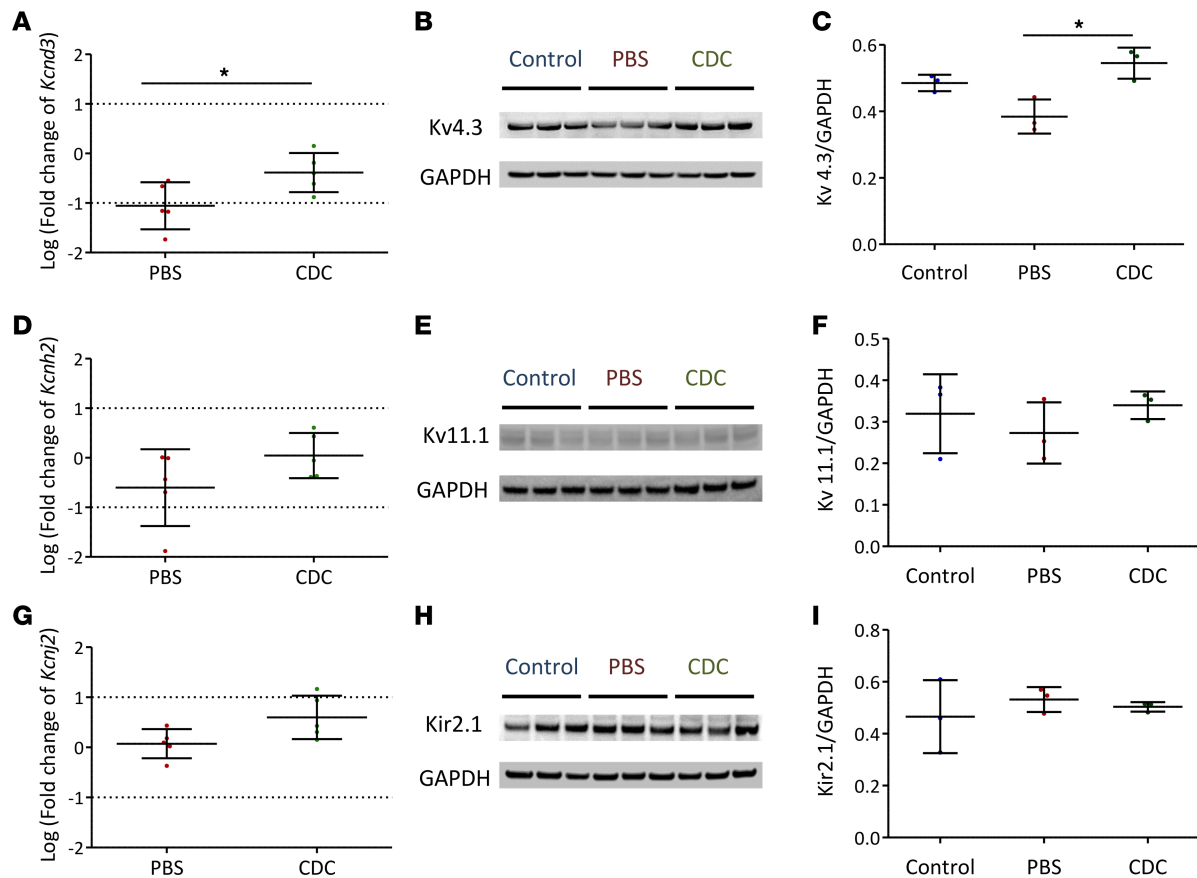


Figure 5. Remodeling of ion channel genes and proteins. (A) The I_{to} -encoding transcript *Kcnd3* was upregulated in CDC-treated rats compared with PBS animals (log[fold change compared to control] -0.39 ± 0.40 in CDCs vs. -1.06 ± 0.47 in PBS, $P = 0.041$). (B) Expression of the I_{to} protein, Kv4.3, was decreased in PBS rats and rescued by CDC treatment. (C) Quantification showed that CDCs upregulate Kv4.3 expression (0.54 ± 0.05 in CDCs vs. 0.38 ± 0.05 in PBS, $P = 0.008$). (D) The I_{kr} -encoding transcript *Kcnh2* was unchanged (log[fold change compared to control] -0.14 ± 0.43 in CDCs vs. -0.49 ± 0.68 in PBS, $P = 0.352$). (E) Western blots showed very heterogeneous but similar expression of the I_{kr} protein, Kv11.1. (F) Expression levels of Kv11.1 were similar in quantification (0.59 ± 0.09 in CDCs vs. 0.62 ± 0.17 in PBS, $P = 0.95$). (G) The I_{k1} -encoding transcript *Kcnj2* was similarly expressed (log[fold change compared to control] 0.60 ± 0.43 in CDCs vs. 0.07 ± 0.29 in PBS, $P = 0.054$). (H) Expression of the I_{k1} protein, Kir2.1, was similar. (I) Quantification of Kir2.1 showed similar expression between the experimental groups (0.50 ± 0.02 in CDCs vs. 0.53 ± 0.05 in PBS, $P = 0.91$). * $P < 0.05$. $n = 5$ for transcript analyses, each group. $n = 3$ for Western blotting, each group. Error line indicates mean and standard deviation. Student's t test was used for A, D, and G. Kruskal-Wallis test was used for C, F, and I.

Transcriptome analyses. Next-generation RNA sequencing in hearts of controls, placebo, and CDC-treated HFpEF rats revealed global changes in gene expression (Figure 7A). Interestingly, CDC therapy rescued the expression levels of more than 300 genes of HFpEF rats toward those of control rats. Some of the important signaling pathways are depicted in Figure 7B. Among those, calcium signaling and tight junction pathways were notably affected by CDC therapy. These include genes relevant to diastolic dysfunction and action potential remodeling (Figure 7C).

Discussion

Here, we have demonstrated antiarrhythmic effects of heart-derived cell therapy in a rodent model of HFpEF (Figure 8). CDCs attenuated inducible VA by shortening APD and increasing APD homogeneity (Figure 8). Upregulation of I_{to} -related transcripts, protein, and ionic currents underlay the CDC-induced abbreviation of APD. Increased homogeneity likely reflects both the upregulation of I_{to} as well as the decrease in fibrosis. Furthermore, CDCs prolonged survival in HFpEF rats, including a decrease in sudden deaths.

HFpEF, once regarded as rare relative to HFREF, is now at least as common, but much more enigmatic in its pathogenesis (5, 17, 18). None of the medications that prolong life in HFREF have been shown to work in HFpEF (7). Sudden death is the leading mode of exodus in HFpEF patients, but the underlying mechanism is unknown (9, 10). The limited data available are consistent with the idea that intrinsic

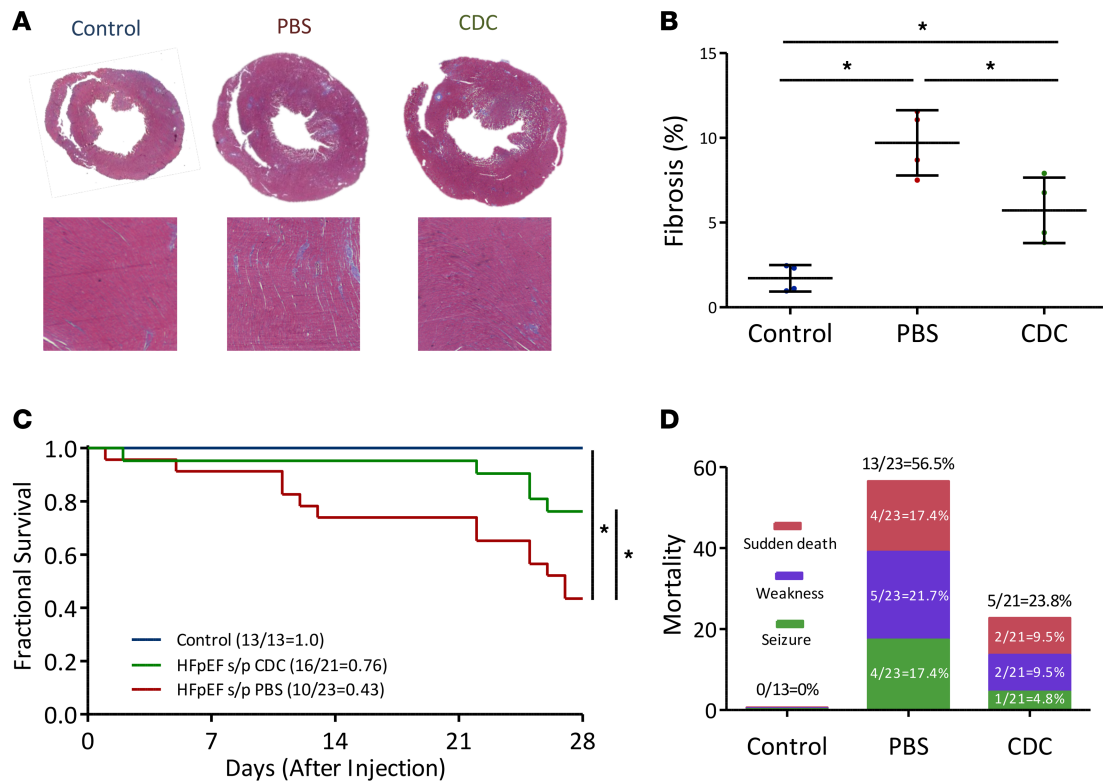


Figure 6. CDCs attenuated fibrosis and prolonged survival in HFpEF rats. (A) Representative Masson's trichrome staining of control, PBS-, and CDC-injected hearts. (B) Fibrosis was significantly reduced in CDC-treated rats compared with PBS-injected animals ($5.7\% \pm 1.9\%$ in CDCs vs. $9.7\% \pm 1.9\%$ in PBS, $P = 0.018$). (C) Survival analysis showed prolonged survival in CDC-treated rats compared with PBS rats (log-rank $P = 0.035$). (D) Cause-of-death analysis showed a trend of decreasing sudden death rate. $*P < 0.05$. Error line indicates mean and standard deviation. $n = 4$ for fibrosis analysis, each group. $n = 13$ in control, $n = 23$ in PBS, and $n = 21$ in CDC for survival analysis. Kruskal-Wallis test was used for B, and log-rank test was used for C.

susceptibility to VA, due to electrophysiological changes at the cellular and organ levels, underlie at least some sudden deaths in HFpEF (12). To test this concept, however, larger-scale prospective studies, with ambulatory electrocardiographic recordings, will be required.

CDCs were first manufactured and identified as cardiac progenitor cells in 2007 (14). However, the therapeutic principles recruited by these cells are now recognized to transcend regeneration to include immunomodulatory, angiogenic, antiinflammatory, and antifibrotic effects (8, 19–22). In any given form of pathology, a subset of these effects may figure most prominently in CDCs' disease-modifying bioactivity. In HFpEF rats, antiinflammatory and antifibrotic effects of CDCs underlie the reversal of diastolic dysfunction; other mechanisms play only a minor role (8). The antifibrotic effects of CDCs in this model have been reported; multiple profibrotic cytokines (e.g., TNF- α , IL-6, MCP-1, and TIMP-1) are overexpressed in HFpEF and decreased after CDC treatment (8). Here, we add reverse electrical remodeling to the effects of CDCs; this antiarrhythmic mechanism underlies the treatment-related decrease in VA, and possibly contributes to the prolongation of survival. The present study further rationalizes translational studies of CDCs in HFpEF, and also provides mechanistic insights into arrhythmogenesis in this poorly understood disease. Delayed repolarization has been postulated to be a cause of VA in HF (23, 24), but successful interventions have been lacking, leading to mechanistic uncertainty. Here, we find that partial correction of the repolarization abnormalities suppresses VA and prolongs survival, adding evidence linking repolarization to HF-related arrhythmias. APD dispersion and fibrosis play important roles as well. Interestingly, CDCs modify all 3 major mechanisms of VA in HFpEF, producing synergistic benefits.

CDCs reverse adverse electrical remodeling by upregulating I_{to} , apparently at the transcriptional level. While elucidating the detailed mechanisms is beyond the scope of this report, CDCs mediate most of their effects via secreted exosomes (25, 26) and their RNA contents (27, 28). Thus, future mechanistic investigation of the VA-suppressive effects of CDCs will logically focus on dissection of CDC exosomes and their contents.

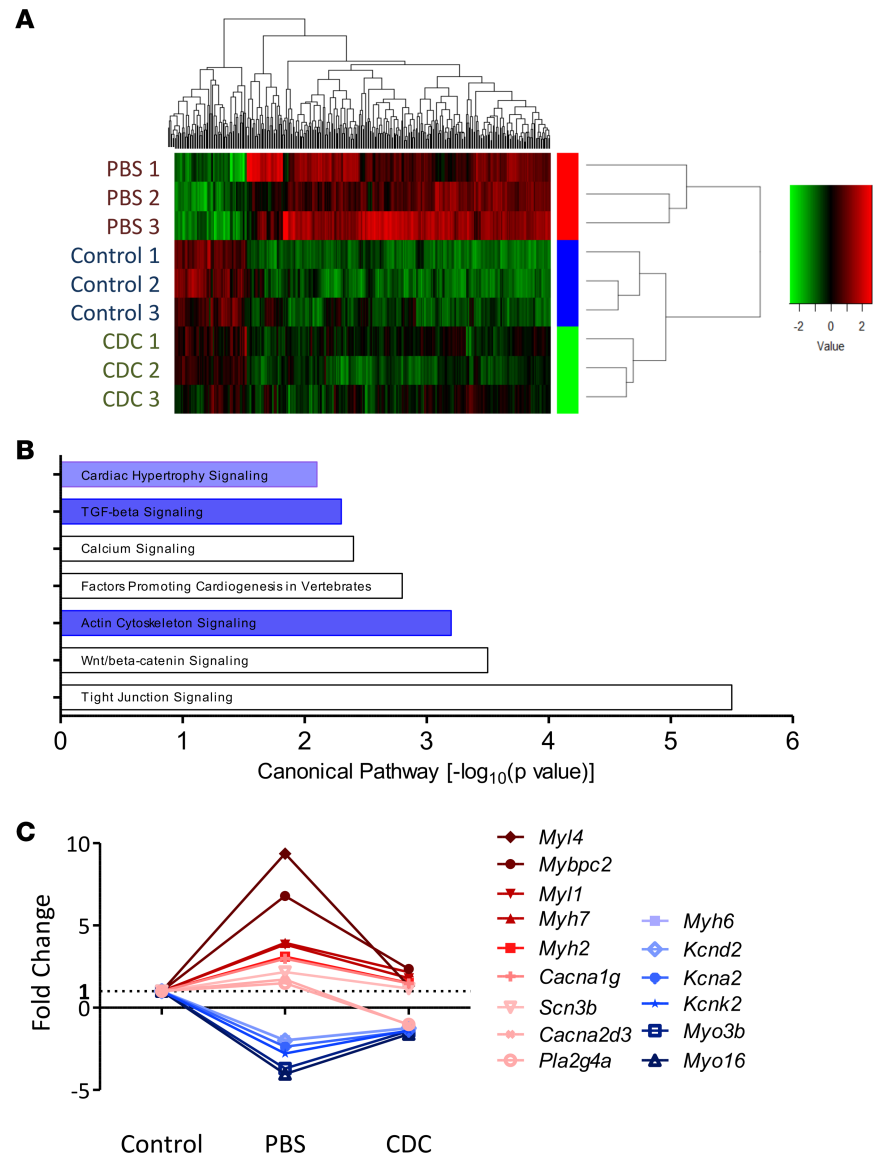


Figure 7. Transcriptomic analyses. (A) Heatmaps show that the phenotypic changes in HFpEF rats affected by CDCs are accompanied by global changes in gene expression. (B) CDC treatment reverted the gene expression patterns of HFpEF rats toward those of control rats; some of the important signaling pathways are depicted (blue, inhibited; white, not clear from the database). (C) Summary changes of genes underlying diastolic dysfunction and action potential remodeling.

Study limitations. Our study has several limitations. First of all, although this is arguably the best-validated preclinical HFpEF model, it does not reflect some of the pathology seen in HFpEF patients. HFpEF is a disease associated with aging, so using young rats might not fully recapitulate the pathology of old hearts. However, the hypertensive phenotype does reproduce another comorbidity associated with human HFpEF. It should also be emphasized that all rats included in this study had phenotypically verified HFpEF by echo. Second, the AI used here to quantify VA is a heuristic concept that is not directly applicable to human studies. Given that AI is heuristic, it is meant simply to stimulate interest as a means of furthering investigation. Directional changes and group distributions are potentially informative, but the absolute values have no intrinsic meaning. Nonetheless, it provides a compact synthesis of the salient responses to PES and thus helps to quantify arrhythmogenicity. Regardless of AI, CDCs were able to reduce the duration of VA, as quantified by the number of VA beats. Third, the electrophysiologic properties of the rat heart are known to be quite different from those of human hearts. Nevertheless, QT prolongation is a feature of human HFpEF (16), hinting at a clinically relevant role for abnormal repolarization. Fourth, we have not established an unambiguous causal role for inducible VA in HFpEF-associated sudden death, nor have we

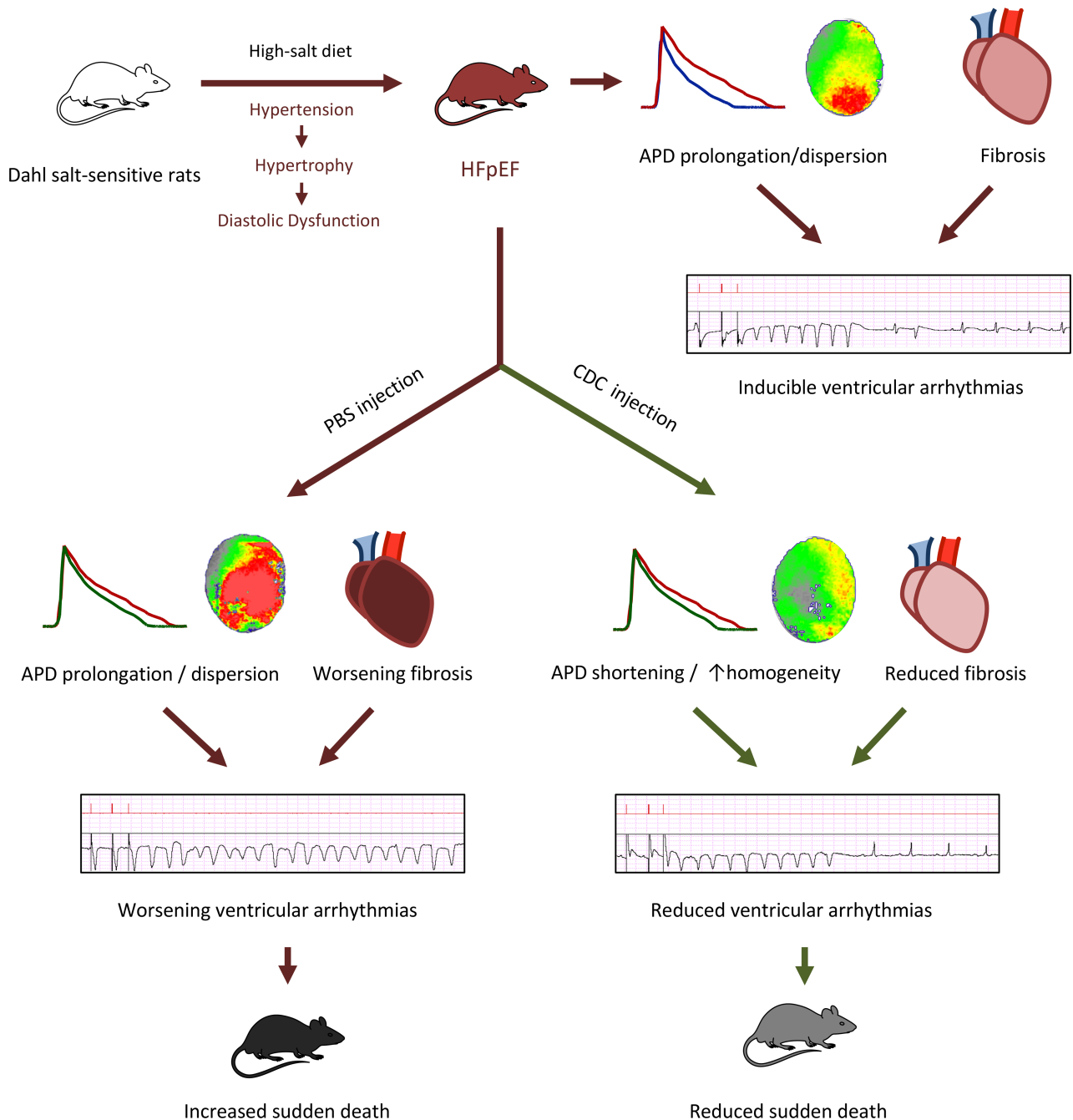


Figure 8. Schematic summary of the study. In this study, we have demonstrated the reverse electrical remodeling of heart-derived cell therapy in a rodent model of HFpEF. CDCs attenuated inducible VA by shortening APD and increasing APD homogeneity. CDCs also reduced fibrosis, which can be potentially antiarrhythmic. The antiarrhythmic effects of CDCs further decreased sudden death risk and improved survival.

documented a statistically significant decrease in sudden death in HFpEF rats treated with CDCs. However, our previous findings that VAs precipitate sudden death (13) suggest that the decreased sudden death risk might be explained by the antiarrhythmic effects of CDCs.

Methods

Rodent HFpEF model. All the rodent protocols and experiments were approved by the Cedars-Sinai Medical Center Institutional Animal Care and Use Committee. A DSS rat model of HFpEF was employed as described previously (8, 12). In brief, male 7-week-old DSS rats (Charles River Laboratories) were fed a HS diet (AIN-76A + 8% NaCl with irradiation, Research Diets) to induce HFpEF (Figure 1A).

DSS rats fed a NS diet (AIN-76A [0.3% NaCl] with irradiation, Research Diets) served as controls. Feeding was continued ad libitum until the end of experiments. At 14–15 weeks of age, transthoracic echocardiography was performed to measure systolic and diastolic function. Echo-verified (diastolic dysfunction with preserved EF) HS-fed rats with signs of HF (decreased activity, weakness, shortness of breath, weight loss or corporal edema) were diagnosed with HFpEF by 14–15 weeks old. PES was applied to measure baseline arrhythmogenicity.

Transthoracic echocardiography. Rats were anesthetized with 2% isoflurane for transthoracic echocardiography (Vevo 3100, VisualSonics). Systolic function was measured by calculating EF (%) from the parasternal short axis view. Diastolic function was checked from the apical 4-chamber view by measuring E/A and E/E' ratios. E and A waves were measured from the pulse wave Doppler mode between the tips of the mitral valve (8, 29–31). E' wave was measured from the tissue Doppler mode at the septal corner of the mitral annulus (29). Color Doppler mode was used to measure diastolic parameters. Three images were averaged.

Programmed electrical stimulation. Rats were induced with 5% isoflurane and then intubated and connected to the mechanical ventilator. Anesthesia was maintained with 2% isoflurane for PES. Core body temperature was kept at 36°C–38°C (rectal) with a heating lamp. ECG was monitored during the procedure with dual bio-amps (AD Instruments). A thoracotomy was performed, the pericardium was excised, and an electrode was placed into the apex. PES was performed using an electronic stimulator (PowerLab, AD Instruments) (12) with a drive train of 10 stimuli (S1, 5 V, 1-ms pulse width, and 100-ms interval), followed by 3 extrastimuli (S2, S3, and S4) (5 V and 1-ms pulse width). To quantify VA inducibility, we implemented an AI defined by the following formula: (number of VA beats + [last extrastimulus coupling interval – 40]) / (square root of [number of extrastimuli]).

Injection of CDCs versus PBS. CDCs were derived from a Sprague Dawley rat (Charles River Laboratories) following standard protocols (Figure 1B). In brief, heart explants were plated on dishes coated with fibronectin. Once confluent after 7–10 days, explant-derived cells were detached with enzymes and cultured in poly-D-lysine-coated plates to support cardiosphere formation. After 3 days, cardiospheres were isolated and then plated on dishes coated with fibronectin. CDCs were subsequently expanded and passages 4 to 6 were used for in vivo experiments. HFpEF rats were randomly assigned (using block randomization method) to allogeneic CDCs versus PBS by intracoronary injection (ventricular cavity injections during aortic cross-clamping for 20 seconds) (8, 32). We used 500,000 CDCs resuspended in 100 μ l PBS (5% heparin and 1% nitroglycerin) versus 100 μ l PBS (5% heparin and 1% nitroglycerin).

Electrocardiography. ECG was recorded during PES with dual bio-amps (AD Instruments). PR interval, QRS width, QT interval, and RR interval were measured and averaged on LabChart 7 software (AD instruments). QTc interval was calculated as QT interval (ms) divided by the square root of the RR interval (seconds) (33).

Ex vivo optical mapping. Rats were anesthetized with 5% isoflurane, euthanized, and the heart was harvested. The ascending aorta was cannulated and retrogradely perfused in a Langendorff apparatus with Tyrode solution (136 mM NaCl, 5.4 mM KCl, 0.33 mM NaH_2PO_4 , 1.0 mM MgCl_2 , 10 mM HEPES, 1.8 mM CaCl_2 , and 10 mM glucose). RH237 (Molecular Probes) was used to measure action potentials (0.05 mg in 50 ml Tyrode solution). Blebbistatin (Sigma-Aldrich) was used as an uncoupler to avoid motion artifacts (0.1 mg in 100 ml Tyrode solution). Images were acquired using a MiCAM05 Ultima-L CMOS camera (SciMedia) with filters (excitation 520/35 nm, dichroic 560 nm, emission 715 nm long-pass). BV-Ana software (SciMedia) was used to calculate APD and dispersion.

Isolation of cardiomyocytes. Rat ventricular cardiomyocytes were isolated for single-cell electrophysiology as described previously (14). In brief, heparin (4,000 IU per kg) was injected intraperitoneally 1 hour prior to harvesting the heart. Rats were euthanized by excising the heart. The heart was cannulated and retrogradely perfused with Ca-free Tyrode solution at 37°C. After 5 minutes of perfusion with Ca-free Tyrode solution, an enzyme solution containing type II collagenase (1.66 mg/ml, Worthington Biomedical) and type XIV protease (0.13 mg/ml, Sigma-Aldrich) in Ca-free Tyrode solution was perfused for 15–25 minutes to digest the heart. Following enzymatic digestion, hearts were perfused with Tyrode solution containing 0.2 mM CaCl_2 for 5 minutes. The left ventricle was excised, minced, and filtered (100 μ m) to isolate ventricular cardiomyocytes for single-cell electrophysiology. Calcium chloride was gradually increased to a final concentration of 1.0 mM.

Whole-cell patch clamp. Isolated cardiomyocytes were placed in an experimental chamber on the stage of a Zeiss Axiovert 200 microscope. Patch electrodes were pulled from borosilicate glass (TW150F-4, World Precision Instruments) on a horizontal micropipette puller (P-97, Sutter Instruments). The fire-polished

electrodes were designed to have a resistance of 1–2 M Ω . An Axopatch 200B amplifier was used under the control of pClamp 10 software and a Digidata 1440A PC interface (all from Molecular Devices). Tyrode solution was superfused at room temperature. I_{to} , I_{Kr} , and I_{K1} were measured using the whole-cell clamp configuration. The external solution contained (in mM) 136 mM NaCl, 5.4 KCl, 0.33 NaH₂PO₄, 1.0 MgCl₂, 10 HEPES, 10 glucose, 1.0 CaCl₂, and 20 μ M nifedipine. Final pH was adjusted to 7.4 by NaOH. The micropipette solution contained (in mM) 5.4 NaCl, 130 KCl, 1.0 MgCl₂, 10 HEPES, 0.05 cAMP, 5 MgATP, and 2.8 phosphocreatine, adjusted to a final pH of 7.2 by KOH. I_{to} and I_{Kr} were evoked by voltage steps from –60 to +60 mV in 10-mV increments lasting 3,000 ms after a 100-ms prepulse to –40 mV to inactivate Na channels. I_{to} amplitude was measured as the difference between the peak outward current and the current at the end of the pulse. E4031 (1 μ M, Sigma-Aldrich) was applied and currents were subtracted to calculate E4031-sensitive current as I_{Kr} . I_{K1} was evoked by voltage steps from –120 to +10 mV in 10-mV increments lasting 500 ms after a 100-ms prepulse. I_{K1} was measured as barium-sensitive current by subtraction (100 μ M). Series resistance compensation (40% to 70%) was used and membrane currents sampled at 5 kHz were filtered at 2 kHz. Current density (pA/pF) was measured from the current amplitude (pA) divided by the membrane capacitance (pF).

Quantitative reverse transcriptase polymerase chain reaction. Heart tissues were stored in Allprotect Tissue Reagent (Qiagen). Total RNA was isolated from the apex using RNeasy Plus Universal Mini Kit (Qiagen) and cDNA was synthesized with 2 μ g of RNA using High Capacity RNA-to-cDNA Kit (Applied Biosystems). Primers were acquired from Abcam (*Kcnd3*, *Kcnh2*, *Kcnj2*, and *Ldha*). Reverse transcriptase polymerase chain reaction was performed with TaqMan Universal Master Mix II with UNG (Applied Biosystems). The following conditions were used: 50°C for 2 minutes (UNG incubation), 95°C for 10 minutes (polymerase activation), and 40 cycles of 95°C for 15 seconds (denaturation) and 60°C for 1 minute (annealing and extension). Cycle threshold (CT) value was standardized to the CT value of *Ldha* (lactate dehydrogenase A). Fold change of the mRNAs was calculated as $2^{-\Delta\Delta CT}$ compared with the control group and log scale of fold change was utilized to compare expression levels of the mRNAs.

Protein isolation and Western blot. Protein was isolated from heart tissues using Tissue Ruptor (Qiagen) with RIPA buffer and protease inhibitor (Thermo Fisher Scientific). Protein was quantified by Bradford Protein Assay (Bio-Rad). NuPAGE system was used for Western blotting (4%–12% Bis-Tris gradient gel, 2-morpholinoethane [MES] sodium dodecyl sulfate [SDS] running buffer, transfer buffer, and Tris-buffered saline [TBS] with Tween) (Life Technologies). Kv4.3 antibody (P0358), Kv4.2 antibody (P0233), and connexin 43 antibody (C6219) were acquired from Sigma-Aldrich. Kv11.1 (ab92513), Kir2.1 (ab109750), Kv1.4 (ab16718), KChIP2 (ab3473), and GAPDH (ab9483) antibodies were obtained from Abcam. Primary antibody (1:200–1:1,000) was incubated overnight with 3% bovine serum albumin at 4°C. Secondary antibody (horseradish peroxidase conjugated, 1: 20,000) was incubated for 90 minutes under 3% bovine serum albumin at room temperature. Immunoreactivity was detected by enhanced chemiluminescent substrate (Thermo Fisher Scientific).

Masson's trichrome staining. Mid-ventricular heart tissues were sectioned and stained per manufacturer's protocol (Sigma-Aldrich). Fractional myocardial fibrosis (blue-gray pixels divided by total pixels) was quantified using ImageJ software (NIH).

Survival analysis. Rats were monitored at the vivarium at least 2 times per day by laboratory staff blinded to experimental group assignment, and followed up to 4 weeks after the injection of CDCs versus PBS. Rats too sick to eat or drink were euthanized by recommendation from laboratory staff per institutional animal welfare policy. Common reasons for protocol-mandated euthanasia were progressive weakness and continuous seizures (all of seizing rats with more than 5 minutes of continuous seizures were euthanized as per the protocol).

Next-generation RNA sequencing. Total RNA was isolated from left ventricular tissue by RNeasy kit (Qiagen). Sequencing was performed with Illumina NextSeq 500 for a single read of 75 runs. Differentially expressed genes were analyzed using the edgeR software. Genes showing altered expression of *P* less than 0.05 with greater than 1.5-fold changes were considered differentially expressed. The pathway and network analyses were performed using Ingenuity Pathway Analysis software (Qiagen).

Statistics. Continuous variables are shown as mean \pm standard deviation (except for I_{to} , I_{Kr} , and I_{K1} densities: mean \pm standard error of mean). Normal distribution was assessed using Kolmogorov-Smirnov test. Homogeneity of variance was tested by Levene's test. Continuous data were tested across groups with ANOVA, or where repeated measures over time with mixed-model regression. Residuals were inspected

to confirm model fit and lack of outliers. Nonparametric testing was performed with Kruskal-Wallis test. Survival times were tested with log-rank test. In all cases, post hoc pair-wise testing was adjusted for multiple comparisons. Fischer's exact test with FDR option was used to calculate the significance of the canonical pathway. For all testing, a 2-tailed *P* value of less than 0.05 was used to determine statistical significance. SAS v9.4 software was used for analysis.

Study approval. All the rodent protocols and experiments were approved by the Cedars-Sinai Medical Center Institutional Animal Care and Use Committee.

Author contributions

JHC performed experiments, analyzed data, and drafted the manuscript. PJK, RZ, RES, EMK, RGR, and GDC performed experiments. CB performed statistical analyses. KL performed experiments and analyzed data. JIG conceived experiments and supervised experiments. EM and EC conceived experiments, supervised experiments, and wrote the manuscript.

Acknowledgments

This research was supported by NIH T32 HL116273, and Department of Defense grant PR150620. General laboratory support was provided by NIH HL 135866 and by the Cedars-Sinai Board of Governors Heart Stem Cell Center. EM is the Mark S. Siegel Family Distinguished Professor of the Cedars-Sinai Medical Center.

Address correspondence to: Eugenio Cingolani, Smidt Heart Institute, Cedars-Sinai Medical Center, 127 S. San Vicente Boulevard, Suite A3600, Los Angeles, California 90048, USA. Phone: 310.248.6679; Email: Eugenio.Cingolani@csmc.edu.

- Kochanek KD, Murphy SL, Xu J, Tejada-Vera B. Deaths: Final data for 2014. *Natl Vital Stat Rep.* 2016;65(4):1–122.
- Shah KS, et al. Heart failure with preserved, borderline, and reduced ejection fraction: 5-year outcomes. *J Am Coll Cardiol.* 2017;70(20):2476–2486.
- Jessup M, Brozena S. Heart failure. *N Engl J Med.* 2003;348(20):2007–2018.
- Writing Committee Members, et al. 2013 ACCF/AHA guideline for the management of heart failure: a report of the American College of Cardiology Foundation/American Heart Association Task Force on practice guidelines. *Circulation.* 2013;128(16):e240–e327.
- Dunlay SM, Roger VL, Redfield MM. Epidemiology of heart failure with preserved ejection fraction. *Nat Rev Cardiol.* 2017;14(10):591–602.
- Redfield MM. Heart failure with preserved ejection fraction. *N Engl J Med.* 2016;375(19):1868–1877.
- Sharma K, Kass DA. Heart failure with preserved ejection fraction: mechanisms, clinical features, and therapies. *Circ Res.* 2014;115(1):79–96.
- Gallet R, et al. Cardiosphere-derived cells reverse heart failure with preserved ejection fraction (HFpEF) in rats by decreasing fibrosis and inflammation. *JACC Basic Transl Sci.* 2016;1(1–2):14–28.
- Zile MR, et al. Mode of death in patients with heart failure and a preserved ejection fraction: results from the Irbesartan in Heart Failure With Preserved Ejection Fraction Study (I-Preserve) trial. *Circulation.* 2010;121(12):1393–1405.
- Vaduganathan M, et al. Mode of death in heart failure with preserved ejection fraction. *J Am Coll Cardiol.* 2017;69(5):556–569.
- Tomaselli GF, Zipes DP. What causes sudden death in heart failure? *Circ Res.* 2004;95(8):754–763.
- Cho JH, et al. Delayed repolarization underlies ventricular arrhythmias in rats with heart failure and preserved ejection fraction. *Circulation.* 2017;136(21):2037–2050.
- Cho JH, et al. Ventricular arrhythmias underlie sudden death in rats with heart failure and preserved ejection fraction. *Circ Arrhythm Electrophysiol.* 2018;11(8):e006452.
- Smith RR, et al. Regenerative potential of cardiosphere-derived cells expanded from percutaneous endomyocardial biopsy specimens. *Circulation.* 2007;115(7):896–908.
- Little WC, Oh JK. Echocardiographic evaluation of diastolic function can be used to guide clinical care. *Circulation.* 2009;120(9):802–809.
- Wilcox JE, Rosenberg J, Vallakati A, Gheorghide M, Shah SJ. Usefulness of electrocardiographic QT interval to predict left ventricular diastolic dysfunction. *Am J Cardiol.* 2011;108(12):1760–1766.
- Kass DA, Bronzwaer JG, Paulus WJ. What mechanisms underlie diastolic dysfunction in heart failure? *Circ Res.* 2004;94(12):1533–1542.
- Borlaug BA. The pathophysiology of heart failure with preserved ejection fraction. *Nat Rev Cardiol.* 2014;11(9):507–515.
- Johnston PV, et al. Engraftment, differentiation, and functional benefits of autologous cardiosphere-derived cells in porcine ischemic cardiomyopathy. *Circulation.* 2009;120(12):1075–1083.
- Malliaras K, et al. Safety and efficacy of allogeneic cell therapy in infarcted rats transplanted with mismatched cardiosphere-derived cells. *Circulation.* 2012;125(1):100–112.
- Malliaras K, et al. Validation of contrast-enhanced magnetic resonance imaging to monitor regenerative efficacy after cell

- therapy in a porcine model of convalescent myocardial infarction. *Circulation*. 2013;128(25):2764–2775.
22. Aminzadeh MA, et al. Therapeutic efficacy of cardiosphere-derived cells in a transgenic mouse model of non-ischaemic dilated cardiomyopathy. *Eur Heart J*. 2015;36(12):751–762.
23. Tomaselli GF, et al. Sudden cardiac death in heart failure. The role of abnormal repolarization. *Circulation*. 1994;90(5):2534–2539.
24. Tomaselli GF, Marbán E. Electrophysiological remodeling in hypertrophy and heart failure. *Cardiovasc Res*. 1999;42(2):270–283.
25. Ibrahim AG, Cheng K, Marbán E. Exosomes as critical agents of cardiac regeneration triggered by cell therapy. *Stem Cell Reports*. 2014;2(5):606–619.
26. Ibrahim A, Marbán E. Exosomes: Fundamental biology and roles in cardiovascular physiology. *Annu Rev Physiol*. 2016;78:67–83.
27. de Couto G, et al. Exosomal microRNA transfer into macrophages mediates cellular postconditioning. *Circulation*. 2017;136(2):200–214.
28. Cambier L, et al. Y RNA fragment in extracellular vesicles confers cardioprotection via modulation of IL-10 expression and secretion. *EMBO Mol Med*. 2017;9(3):337–352.
29. Liu J, Rigel DF. Echocardiographic examination in rats and mice. *Methods Mol Biol*. 2009;573:139–155.
30. Doi R, et al. Development of different phenotypes of hypertensive heart failure: systolic versus diastolic failure in Dahl salt-sensitive rats. *J Hypertens*. 2000;18(1):111–120.
31. Klotz S, Hay I, Zhang G, Maurer M, Wang J, Burkhoff D. Development of heart failure in chronic hypertensive Dahl rats: focus on heart failure with preserved ejection fraction. *Hypertension*. 2006;47(5):901–911.
32. Altman DG, Bland JM. How to randomise. *BMJ*. 1999;319(7211):703–704.
33. Roguin A. Henry Cuthbert Bazett (1885-1950)—the man behind the QT interval correction formula. *Pacing Clin Electrophysiol*. 2011;34(3):384–388.